doi:10.2533/chimia.2012.44 Chimia 66 (2012) 44–51

Electrochemical Scanning Tunneling Microscopy

Knud Gentz[a] and Klaus Wandelt*[ab]

Abstract: The electrochemical scanning tunneling microscope was the first tool for the investigation of solid–liquid interfaces that allowed *in situ* real space imaging of electrode surfaces at the atomic level. Therefore it quickly became an important addition to the repertoire of methods for the determination of the local surface structure as well as the dynamics of reactions and processes taking place at surfaces in an electrolytic environment. In this short overview we present several examples to illustrate the powerful capabilities of the EC-STM, including the observation of clean metal surfaces as well as the adsorption of thin metal layers, specifically adsorbed anions and non-specifically adsorbed organic cations. In several cases the electrode potential has a significant influence on structure and reactivity of the surface that can be explained by the observations made with the EC-STM.

Keywords: Anion adsorption · Electrochemistry · Metal electrodes · Scanning tunneling microscope · Solid–liquid interface

1. Introduction

The scanning tunneling microscope (STM), invented by Binnig and Rohrer[1,2] in the early 1980s, advanced quickly to a standard method for local surface analysis with atomic resolution. However at first it was only applied to surfaces at solid–gas interfaces under vacuum conditions. Yet, many highly interesting phenomena and industrially relevant processes occur at solid–liquid interfaces: corrosion of metals, etching of silicon wafers and production of microprocessors and integrated circuits, various biological processes, heterogeneous catalysis and the power generation in fuel cells to name only a few. For continuous improvements of the technical applications of these processes a detailed understanding of the involved reactions needs to be achieved with the same precision as we are used to from UHV surface science. This creates the need for *in situ* methods which provide information about interfaces between two condensed phases, *i.e.* the solid and the liquid, in general, and possibly down to atomic resolution in particular. Specifically, scanning probe techniques fulfill both conditions, and it was, thus, only four years after its invention that the first report of an STM working in liquids was published.[3] The liquids used for these first experiments were oil and liquid nitrogen, but only one year later Sonnenfeld *et al.* were able to achieve sufficient control to gather structural information of a graphite surface and gold films on a glass substrate in water and water-based electrolyte solutions.[4]

These early experiments however consisted only of a two-electrode setup (tip and surface electrode) and, therefore, lacked the capability to control the electrode potential with respect to a known reference. Since the tip acts also as an electrode in this setup polarization effects and electrochemical charge-transfer reactions can occur at the tip. In order to maintain well-defined and stable tip properties, which is a prerequisite for STM work, destructive reactions at the tip should be avoided or minimized. In 1988 Siegenthaler and coworkers proposed a method for adjusting the electrode and tip potentials independently by combining the tip and work electrode (sample) with an unpolarizable reference electrode (in this case Ag/AgCl) to a three-electrode setup and controlling both potentials with a bipotentiostat.[5] Shortly afterwards Itaya *et al.* published a circuit design in which they added a counter electrode, commonly used in electrochemical measurements, to a four-electrode setup.[6] This configuration allowed the authors to continue scanning during potential changes of the sample and to observe the ongoing Ag deposition on an HOPG crystal, providing for the advancement to a true *in situ* EC-STM. Since then several other groups have entered the field of electrochemical scanning tunneling microscopy (especially the pioneering work of Bard,[7,8] Behm,[9,10] Endres,[11] Ertl,[12,13] Kolb,[10,14] Magnussen,[10,15,16] Soriaga,[17] Wandelt,[18,19] Wandlowski,[20] Weaver[21]) and the range of possible electrolytes was increased to include ionic liquids.[21] Recently, the increase in computing capacity and microprocessor technology allowed even very fast data acquisition. Magnussen and coworkers built a video STM which reaches frame rates of 10 to 30 images per second.[15]

2. What's Different in the Electrolyte?

In all electrochemical STM experiments, tunneling and faradayic currents through the tip are superimposed and cannot be distinguished by the STM controller. To be able to detect tunneling currents within the background and to minimize the noise on the measured signal faradayic currents through the tip as well as currents induced by external influences have to be minimized. The first part can be accomplished by largely insulating the tip electrode, which is commonly done by one of a number of alternative methods, such as coating by apiezon wax and organic polymers (*e.g.* hot glue) or encasing the tip in glass.[22] In order to reduce currents induced by external electromagnetic interference, a shielding by aluminum has been introduced.[5]

2.1 *Sample Preparation*

A second experimental challenge for an electrochemical STM is the preparation of reproducibly well-defined sample surfaces since the usual preparation methods

*Correspondence: Prof. Dr. K. Wandelt[ab]
[a]Institute of Physical and Theoretical Chemistry
University of Bonn
E-mail: k-wandelt@uni-bonn.de
Wegelerstr. 12, D-53115 Bonn, Germany
[b]Institute of Experimental Physics
Plaza Maxa Borna 9, 50-204 Wroclaw, Poland

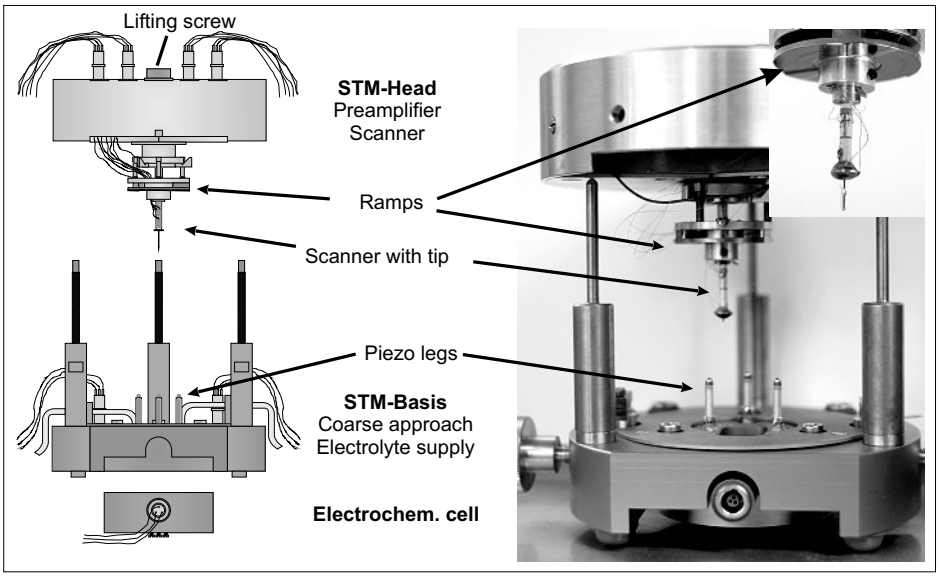

Fig. 1. Schematics and photograph of the Bonn electrochemical STM.

such as inert gas sputtering and annealing employed in UHV are commonly not available except in complex systems which permit direct sample transfer between UHV and EC-STM without contact to air. Therefore alternative sample preparation strategies have to be used for EC-STM.

2.1.1 *Flame Annealing*

A convenient way to prepare noble metal single-crystals is *flame annealing*. In this process the sample surface is exposed to a butane–air flame and heated to a slight reddish hue. This removes organic contaminants by oxidation and heals surface defects. Clavilier, who was the first to propose this method, subsequently quenched the Pt sample in water.[23] A less drastic method is to cool the crystal slowly in an argon flow to room temperature over the course of 15 minutes. This has been successfully shown for Au single crystal samples.[24,25]

2.1.2 *Electrochemical Etching*

Less noble, but technologically more important metal surfaces such as Cu or Fe are susceptible to oxidation under flame annealing conditions. These surfaces may be prepared by electrochemical etching, *i.e.* the sample is immersed in an etching electrolyte and cleaned by anodic dissolution under carefully controlled current and potential conditions. To avoid oxidation during the transfer into the electrochemical cell the sample is protected by a drop of deaerated electrolyte.

2.1.3 *UHV-EC Transfer*

A standard method of surface preparation in a UHV environment is sputtering with Ar-ions and subsequent annealing. A huge advantage of this form of preparation is that the cleanliness of the surface can be verified and its structure characterized by standard UHV analysis methods like low-energy electron diffraction (LEED) or photoelectron spectroscopy. From UHV the sample can then be transferred *via* special buffer chambers to the EC chamber, which is usually kept under argon atmosphere to avoid oxidation of the sample.

2.2 *Tunneling through an Electrolyte*

The fundamentals of tunneling through an electrolyte solution are still not completely understood and descriptive theories are being developed further. A number of aspects differing from tunneling processes in vacuum have to be considered for an understanding of the processes involved. Experimentally, tunnel barriers are found to be significantly lower compared to those in vacuum. One explanation for this effect is that the work function of metals is lowered by the adsorption of water. Moreover, the barrier height is not constant along the surface but modified by an oscillating two-dimensional network of maxima and minima of the potential energy surface due to the distribution and movement of hydrogen and oxygen atoms in the water molecules.[26] The time spent by an electron tunneling through an assumed tunnel gap of 10 Å, is at least two orders of magnitude faster than the motion of molecules[27] so that for an individual tunneling event the barrier can be assumed to be static. For an STM experiment, however, the computing capabilities of the controller limit the speed of information processing and the movement of the tip along the surface is again several orders of magnitude slower than the movement of water molecules. Therefore, the influence of the water layer between tip and surface should average and have no significant influence on the recorded tunneling current. On the other hand the dependence of the tunneling current on the distance between tip and sample does not simply follow an exponential decay as in UHV. Instead several groups have detected a distinct modulation along the surface normal by conducting distance tunneling spectroscopy.[28,29]

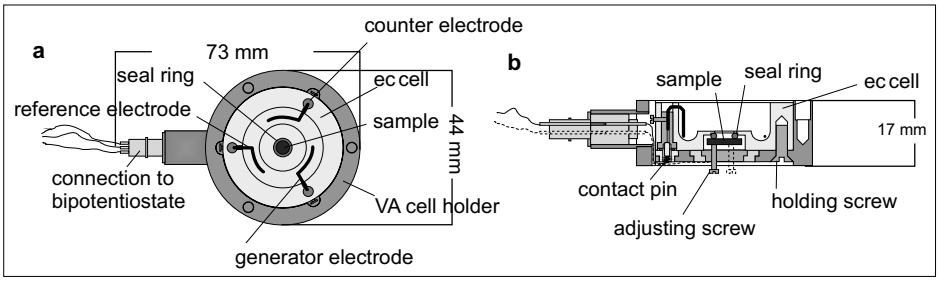

Fig. 2. Sketch of the cell holder and cell.

3. Case Studies

3.1 *The Instrument*

We have selected a wide range of studies in order to demonstrate the capabilities of a scanning tunneling microscopy in an electrochemical environment. Most of the studies have been conducted in a home-built EC-STM developed in Bonn.[18] It consists of a single-tube scanner[30] in a first-order z-drift compensated assembly of a modified Besocke-type[31] STM as shown in Fig. 1. The electrochemical cell can be mounted into the base part of the system. The cell holder allows a variable connection of electrodes. Apart from the sample, which is connected to virtual ground potential, a counter electrode, an internal reference electrode and a generator electrode for *in situ* dissolution of metals into the electrolyte can be connected (see Fig. 2). The base carries also the electrolyte flow system and the three piezos for the coarse approach. An external reference electrode can be connected *via* a Luggin capillary. The STM head (Fig. 1) rests on three spacer bolts and contains the scanner and the preamplifier for the tunneling current. The whole system is mounted on a stack of three brass plates separated by rubber spacers in an aluminum casing. This complete setup rests on a rubber mat on a granite slab, which is suspended from the ceiling by springs for vibrational damping. This design offers some key advantages

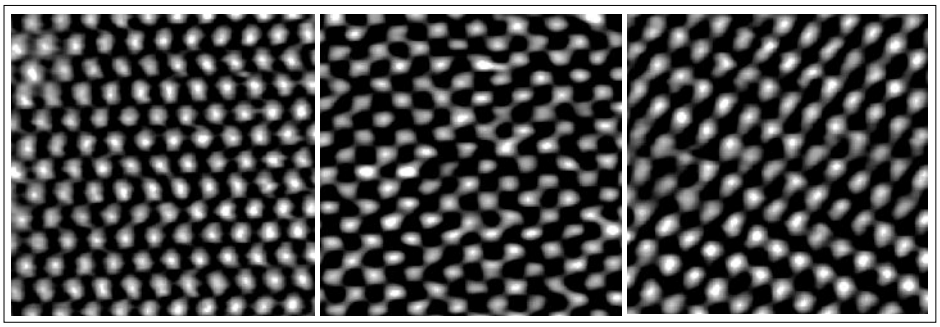

Fig. 3. STM images of the *bare* Cu(111), Cu(100), and Cu(110) electrode surfaces in aqueous electrolyte solution.[32]

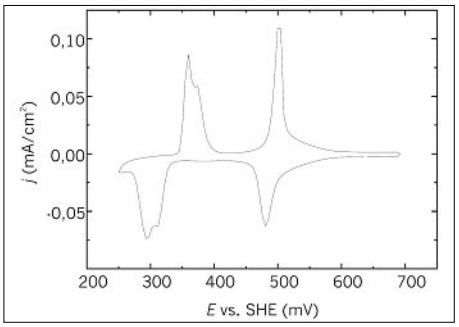

Fig. 4. Cyclic voltammogram of the underpotential deposition of copper on a Au(111) surface.[37]

over commercially available instruments:

• The compact construction of the Besocke-type[31] STM reduces vibrational sensitivity, and the fact that the single-tube scanner and the three piezo legs for the coarse approach are made from identical piezoceramics, provides a first-order thermal z-drift compensation.

• Despite the compact setup the electrochemical cell contains a volume of about 2.5 ml, which is sufficiently large to allow a Nernst diffusion layer to build and to avoid concentration changes due to evaporation. Therefore, electrochemical studies, such as cyclic voltammetry, can be carried out in the same cell as the STM measurements. The sample is fixed against a cut-out in the cell bottom so that only a defined area of the single-crystal surface of the sample is in contact with the electrolyte.

• The electrolyte feed and drain system allows the electrolyte to be changed without removing the scanner or even opening the aluminum casing, greatly increasing experimental flexibility and limiting contamination. The casing also allows air-free operation under inert gas atmosphere.

• The preamplifier is included in the STM head, very close to the tunneling tip. Both are further shielded from electromagnetic interference by aluminum in order to minimize the noise on the tunneling current signal.

• A bipotentiostat independently controls the potential of the tip and the sample versus the reference electrode, allowing potentiodynamic measurements in which the working electrode potential is changed during an ongoing STM scan. Another option is to change the bias potential independently from the sample, which allows tunneling spectroscopy measurements.

A detailed description of the system including the electronic setup of the STM controller has been published in ref. [18].

3.2 *Surface Structure*

In the potential range where no specific adsorption occurs on the electrode surface the atomic structure of the bare surface can be imaged with atomic resolution comparable (or even better than) to UHV. As an example Fig. 3 shows clearly the hexagonal, quadratic and rectangular symmetry of the bare and unreconstructed Cu(111), Cu(100) and Cu(110) surface in contact with the electrolyte.[33–35] In turn, Au- and Pt-single crystal surfaces in aqueous solution show the same reconstructed superstructures as known from UHV. Unlike in UHV, however, in solution their structural transitions are reversible, depending on the electrode potential; a feature unique to the electrolyte interface.[36]

3.3 *Metal Underpotential Deposition*

The structure and the growth phenomena of thin metal films from gas-phase deposition have been intensively studied in UHV. However, the technologically more important route is the electrochemical deposition of metals from an electrolyte solution, where the conditions are certainly different. Especially the deposition of a single monolayer or submonolayer of a metal on an unlike metal surface at potentials above the bulk deposition potential (underpotential deposition UPD) is a unique feature of electrochemical deposition. For instance, the electrodeposition of a copper monolayer on a Au(111) electrode gives a cyclic voltammogram (CV) which shows two distinct copper deposition peaks at a potential more positive than that of the bulk reduction (Fig. 4[37]). The structure present on the surface after passing the more anodic peak, has been a topic of research for some years[38] before Behm and coworkers were able to obtain the first atomically resolved real-space local probe images[39] of the suspected ($\sqrt{3}\times\sqrt{3}$)R30°-Cu superstructure reported in earlier literature. Later, however, *in situ* X-ray diffraction experiments proved that the $\sqrt{3}$-structure is that of sulfate anions coadsorbed in an otherwise pseudomorphic (1×1) Cu monolayer.[40,41] Similarly, the deposition of a Cu UPD monolayer on Au(100) leads to the formation of a pseudomorphic (1×1) superstructure.[42] The reconstruction observed on both Cu-free gold surfaces is lifted by the deposition of the Cu monolayer.[42] A quasi-hexagonal structure observed in earlier experiments[39] for Cu/Au(100) could be explained by the authors with trace amounts of chloride contamination. If, after the completion of the UPD monolayer, the potential is increased again without reaching the anodic dissolution potential of the copper layer, a new phase is found in recent experiments.[43] In this phase the outer two of any group of three copper atom rows move slightly closer together leading to the formation of a striped phase with a commensurate c(3×1) unit cell.

3.4 *Anion Adsorption*

A first reaction step for many electrochemical processes such as corrosion, deposition or catalysis is the adsorption of ions from the electrolyte on the electrode surface. Since these ions are never present without their respective counter ions it is important to gain insight in the influence of these counter ions on the process under investigation. While spectroscopic and electrochemical methods average over the properties of the whole surface, the EC-STM can add high resolution information about the local structure and adsorption processes on an atomic or molecular level.

A basic concept of the solid–liquid interface is the model of the electrochemical double layer which is depicted in Fig. 5 for an electrode at positive potential (with respect to the reference potential). Anions adsorb on the electrode surface, either strongly, in direct contact with the surface (losing at least part of their hydration sphere; inner Helmholtz plane), or weakly, with intact hydration sphere (outer Helmholtz plane). EC-STM provides insight into the structure of the adsorbed anion layer, *e.g.* as a function of electrode potential.

3.4.1 *Anion Layers on the Cu(111) Surface*

The cyclic voltammogram (CV) of a Cu(111) surface in dilute hydrochloric acid shows a pair of current peaks in addition to the copper dissolution and hydrogen evolution reaction signals at either end of the CV. In the range positive of the anodic

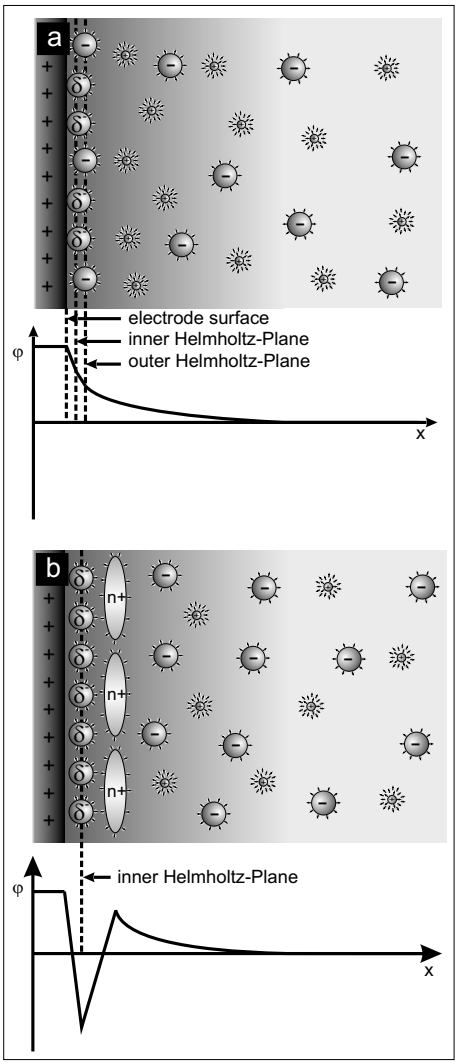

Fig. 5. Simple Grahame model of the electrochemical double layer (a) and adsorption of organic cations after a charge reversal due to a full monolayer of specifically adsorbed anions (b).

peak chloride is adsorbed in a highly ordered (√3×√3)Cl superstructure parallel to the surface while the chloride desorption at negative electrode potentials gives rise to a cathodic peak below which only the bare Cu(111) surface can be observed. An intuitive approach to gaining insight in the structural relation between adsorbate and substrate is to take an image of the adsorbate-covered surface, change the potential to a regime negative of the desorption peak, and then take another image of the adsorbate-free surface. A half-transparent overlay of the two images can then be used to correlate both structures. The problem with this approach, however, is that while the topology of both lattices can be compared with satisfactory accuracy, the exact atom position can deviate due to thermal drift between the two images. This problem can be circumvented by exploiting the spectroscopic capabilities of the STM. If both the adsorbate and the substrate have a density of states near the Fermi energy they can both contribute to the total STM signal. Thus, by varying the bias potential it is possible to obtain an STM image that is either dominated by substrate states or adsorbate states. If the bias voltage is chosen so that both layers contribute to a composite image it is possible to separate the different periodicity of the lattices by Fourier transformation (see Fig. 6[44]). Since the separated images were obtained simultaneously with exactly the same tip position during the scan, their superposition unambiguously shows the relative atom positions of adsorbate and substrate. The results obtained by this approach confirm the assumption that the chloride ions are adsorbed in three-fold hollow sites on the Cu(111) substrate, like in UHV.

Iodide also forms an ordered monolayer on the Cu(111) surface. But this layer is commensurate only at very negative potentials near the onset of the hydrogen evolution reaction where it forms a (√3×√3)R30°-I overlayer. If the potential is increased the iodide layer starts to compress in one direction and forms an uniaxially incommensurate layer (*electrocompressibility*). As a consequence the STM images start to show a one-dimensional long-range height modulation with a wavelength λ that decreases as a function of the applied electrode potential[45] (Fig. 7[45,46]). The ideal hexagonal lattice of the commensurate (√3×√3)R30° structure becomes distorted in the direction of the compression while in the perpendicular direction the iodide overlayer remains in registry with the substrate structure. The reduced symmetry of the compressed adlayer causes the appearance of rotational domains which are indeed observed in the STM images at rotation angles of 120°. Discontinuities in the iodide lattice indicate that the compression does not occur in a uniform way and continuously with the applied potential but by the insertion of super-heavy domain walls (shdw) followed by a relaxation of the iodide layer.[45]

The Cu(111) surface in contact with dilute sulfuric acid represents a particular interesting case. Fig. 8a[18] shows the cyclic voltammogram for this system: Note the large hysteresis between the SO_4^{2-}-adsorption (at –0.55 V) and SO_4^{2-}-

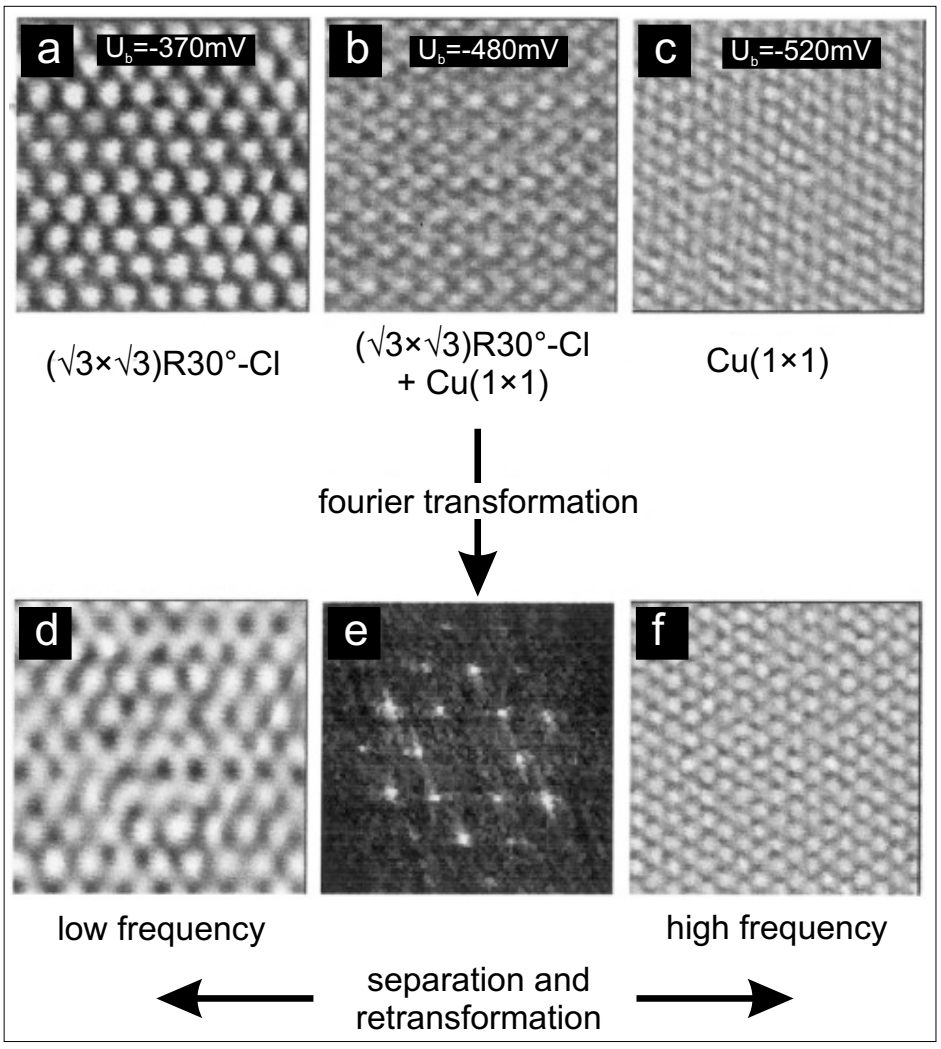

Fig. 6. High-resolution STM images (3.8 nm × 3.8 nm, IT = 18 nA, Ework = –550 mV) of the chloride adlayer (a) and the copper substrate (c). The composed image (b) has been separated into the contributions of substrate and adsorbate by Fourier analysis.[44]

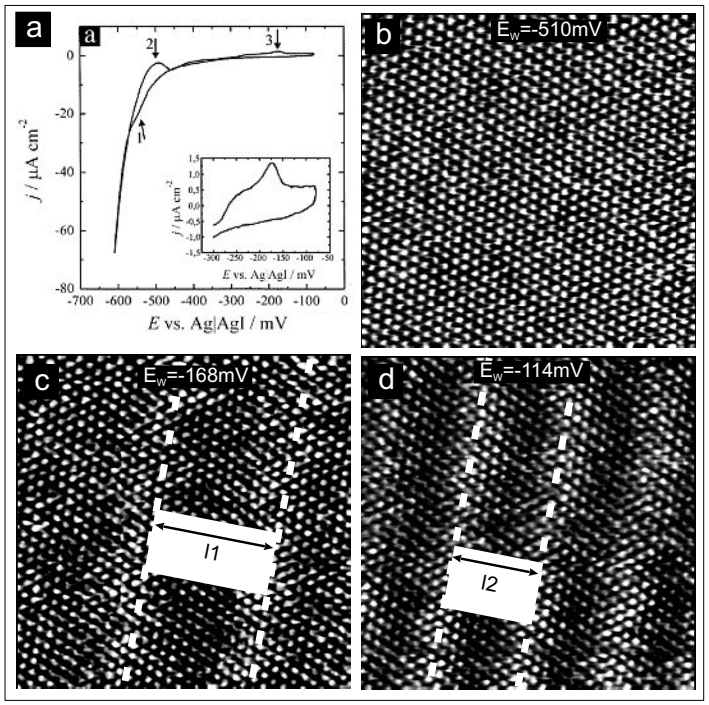

Fig. 7. Cyclic voltammogram of a Cu(111) surface in 0.1 mM KI, 10mM $HClO_4$,[45] dE/dt = 10 mV/s (a), commensurate and electrocompressible uniaxially incommensurate iodide adlayers; (b–d: 13.6 nm × 13.6 nm, b: IT = 1 nA, Ub = 14 mV, c,d: IT = 2,6 nA, Ub = 2 mV).[46]

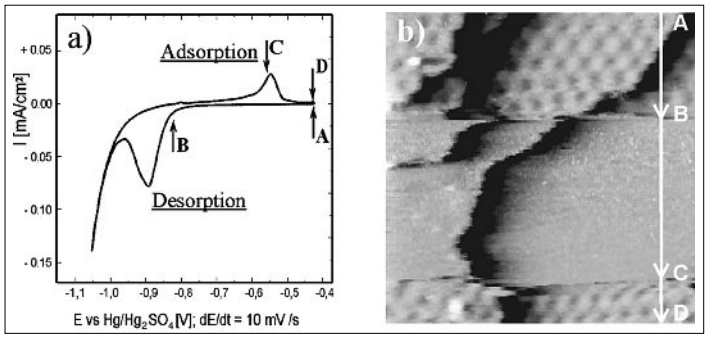

Fig. 8. Cyclic voltammogram (a) of the Cu(111) surface in 5 mM H_2SO_4, STM image recorded during the CV (b: 39 nm × 39 nm, It = 1 nA), the lettered points in the image coincide with those in the CV.[18]

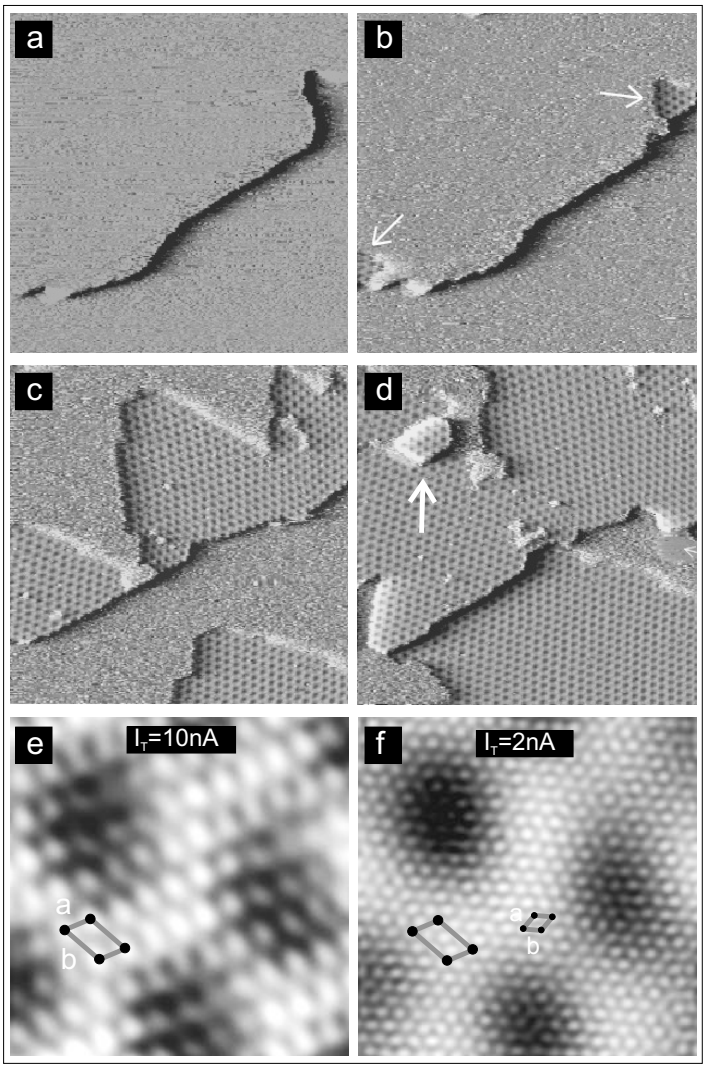

Fig. 9. Slow development of the surface reconstruction and sulfate adsorption (a–d: 101 nm ×101 nm, IT = 1 nA, Ub = 169 mV), high-resolution images of the sulfate (e) and the topmost copper (f) structure (5.9 nm × 5.9 nm, Ub = –2 mV, EW = 100 mV vs. RHE) (a–d),[47] (e–f).[33]

desorption peak (at –0.9 V). In this case the capability of the STM to take images at an arbitrary point of or even during the recording of a voltammogram can help with the assignment of the various peaks to the surface processes that are taking place. The STM image in Fig. 8b was taken during a full voltammetric cycle, starting at point A in the CV and showing a hexagonal Moiré superstructure with a periodicity length of approx. 3 nm. After the point B is passed the surface appears smooth until the Moiré structure reappears at point C. Although the changes in the image are a combination of temporal and spatial/structural changes taking place on the surface, the correlation of the points B and C in the voltammogram to the phase change of the surface structure seems nonambiguous. Such measurements can even give insight in the kinetics of phase transitions. The lifting of the hexagonal phase in Fig. 8 for example seems to be faster (occurring over a smaller number of image lines from left to right) than its re-emergence, hinting at a kinetic hindrance of the Moiré formation. This can, in fact, be tested directly by varying the potential scan rate. For instance, after a sudden potential jump from B to D the Moiré structure is very badly ordered and shows a very high domain density. Conversely, if the potential is increased very slowly the Moiré becomes not only very well ordered, but its emergence can be clearly followed over several minutes (Fig. 9a–d[47]). The comparison of the adsorbate and substrate lattice shows that SO_4^{2-}-anions adsorb in a superstructure similar to what was known from the adsorption of sulfate on the (111) surfaces of Au, Pt, Pd, Ir and Rh. None of the other surfaces, however, shows a hexagonal Moiré superstructure. Surprisingly, the absolute lengths of the unit vectors of the SO_4^{2-} structure (as read from the real space STM images) indicate incommensuracy with the known Cu(111) lattice mesh, instead they correspond to the commensurate SO_4^{2-} structure on Rh. Taking again advantage of the spectroscopic mode of the EC-STM it could be shown that, in fact, the SO_4^{2-} adlayer is not incommensurate with the Cu(111) surface, but that, instead, the strong SO_4^{2-}–Cu interaction leads to a reconstruction of the first Cu atom layer, more precisely, to an expansion to a Cu–Cu interatomic distance similar to that of Rh. Fig. 9e and f[33] show STM images of the same SO_4^{2-}-covered surface area taken with different tunneling parameters. While Fig. 9e is dominated by the SO_4^{2-} overlayer, Fig. 9f represents the lattice of the first Cu layer in direct contact with the SO_4^{2-} anions. The interatomic distance in the latter image is, indeed, 6% larger than within the SO_4^{2-}-free Cu(111) surface (at negative potentials) and thereby similar

to the interatomic distance of a Rh(111) surface. This is direct proof of the SO_4^{2-}-induced expansion of the first Cu layer. As a consequence of this expansion, which corresponds to a lowering of the areal Cu density, Cu atoms are displaced out of the original surface layer, leading to the formation of islands (see arrow in Fig. 9d), that are again SO_4^{2-} covered. And it is this mass transport/displacement which explains the slow kinetics of the Moiré formation, and, thus, the large hysteresis between adsorption and desorption peaks in the cyclic voltammogram.

3.4.2 *Adsorption of Sulfide on a Cu{111}c(2×2)Cl Surface*

A very interesting and important contribution to the field was the development of an *in situ* video STM, which allows direct access to kinetic parameters of surface processes. Magnussen and coworkers were able to observe the diffusion of individual sulfide anions at low coverage over a c(2×2) adlattice covering a Cu(100) single crystal surface almost in real time. The strongly adsorbing sulfide is able to displace adsorbed chloride from the surface so that individual ions are imaged as bright dots on the uniform chloride adlayer (Fig. 10[15]). The corrugation potential of the Cu(100) surface is high enough that under these conditions the image rate of 10–30 Hz is sufficient to observe the S_{ads} hopping frequency and width. By varying the temperature and electrode potential and measuring changes in the hopping rate which was then applied to a 2D continuous time random walk model they were able to deduce kinetic parameters like the activation energy (diffusion barrier) and the pre-exponential factor (attempt rate) which was of the order of vibrational frequencies of the adsorbate.[15]

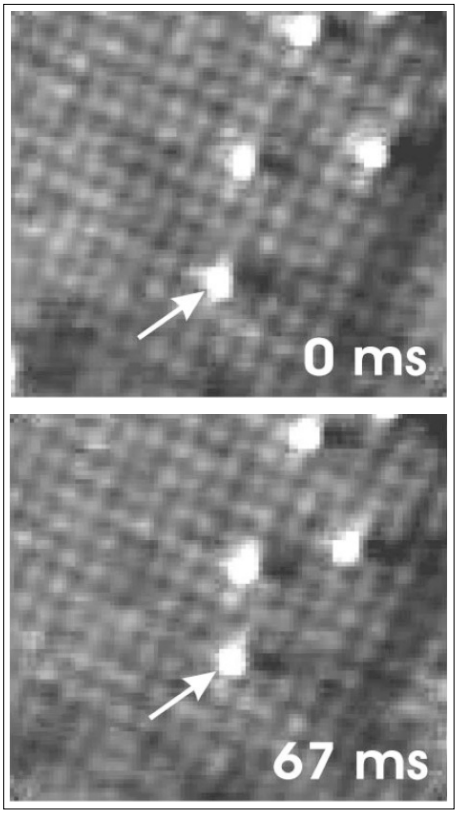

Fig. 10. Successive STM images showing the diffusion of low-coverage sulfide atoms on a c(2x2)-Cl layer on Cu(100) (4 nm × 4 nm, EW = –320 mV vs. SCE).[15]

3.5 *Copper Corrosion in the Presence of Adsorbed Anions*

Iodide adsorbs also on a Cu(100) surface in an incommensurate electro-compressible c(p×2) structure. The p vector decreases with increasing electrode potential until at +80 mV vs. RHE the maximum surface coverage is reached[48] (Fig. 11a,[34] phase I). At this point a local dissolution of the copper starts at step edges, which become increasingly rough (Fig. 11a and b), and a two-dimensional CuI adlayer forms on top of the iodide-covered copper surface[34] (Fig, 11b and c[46]). In the initial stage of the growth process the transient phase II is formed, which is characterized by a wide height modulation that runs at various angles along the surface. With increased coverage of the 2D layer the CuI structure changes to that of the phase III, where the modulation waves are closer and, due to the square substrate lattice, run along directions ±8° off the close-packed iodide rows. The modulation height of only 0.02 nm can clearly be resolved in the STM image (Fig. 11d). By changing the potential the CuI adlayer can again be correlated with the substrate lattice, the crystallographic directions of which are also indicated in Fig. 11d.

3.6 *Adsorption of Organic Cations*

Organic cations are electrostatically repelled by a positively charged electrode surface. The negative charge on specifically adsorbed anions, however, is able to reverse the polarity of the electrode surface in contact with the solution. That way it is possible to stabilize organic cations at the electrode surface that otherwise would not adsorb in a well-ordered structure, if at all (*c.f.* the model in Fig. 5b). In the case of redox-active molecules the electrode potential can be varied to reduce or oxidize the organic cations (Fig. 12a), and to observe concomitant structural changes (Fig. 12b to d). If at electrode potentials more positive than 600 mV vs. Ag/AgCl a Cu(100) electrode is brought into contact with a 10mM HCl solution containing 0.1mM (1,1')dibenzyl(4,4')bipyridinium-(dibenzylviologen-) cations the surface is not only covered with a c(2×2) chloride layer but also with a regular pattern of square shaped moieties (Fig. 12b and c). An enlarged image reveals that these are cavitands with a diameter of 1.1 nm, which are composed out of four individual DBV cations showing an either left- or right-handed arrangement (close-up in Fig. 12c and model in Fig. 12e). This arrangement is the reason for a rotational chirality of the cavitands. Since both, the copper surface as well as the c(2×2)Cl structure adsorbed on top of it, are achiral, two mirror domains of the cavitand phase should be observed on the surface, which is indeed the case (Fig. 12b). By varying the tunneling parameters it is again possible to observe the chloride structure underneath the cavitand phase. In the case of organic cations however, the change in bias voltage not only

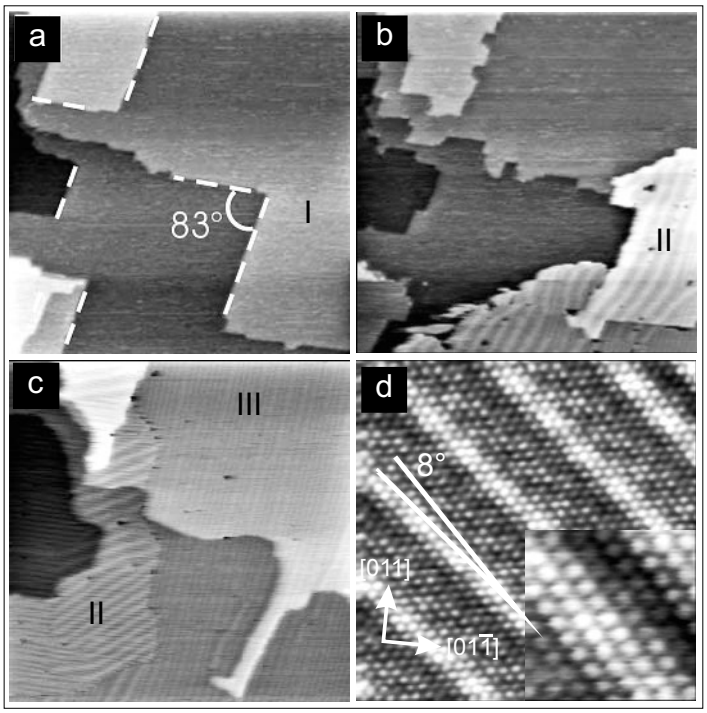

Fig. 11. Stages of the dissolution of Cu(111) and formation of a 2d CuI film (a–c: 108 nm × 108 nm, EW = +120 mV, IT = 0.25 nA, Ub = 224 mV), detail of the atomic structure (d: 12 nm × 12 nm, EW = +120 mV, IT = 1.3 nA, Ub = 10 mV, with 3 nm × 3 nm inset). [a,b,d,[34] c.[46]

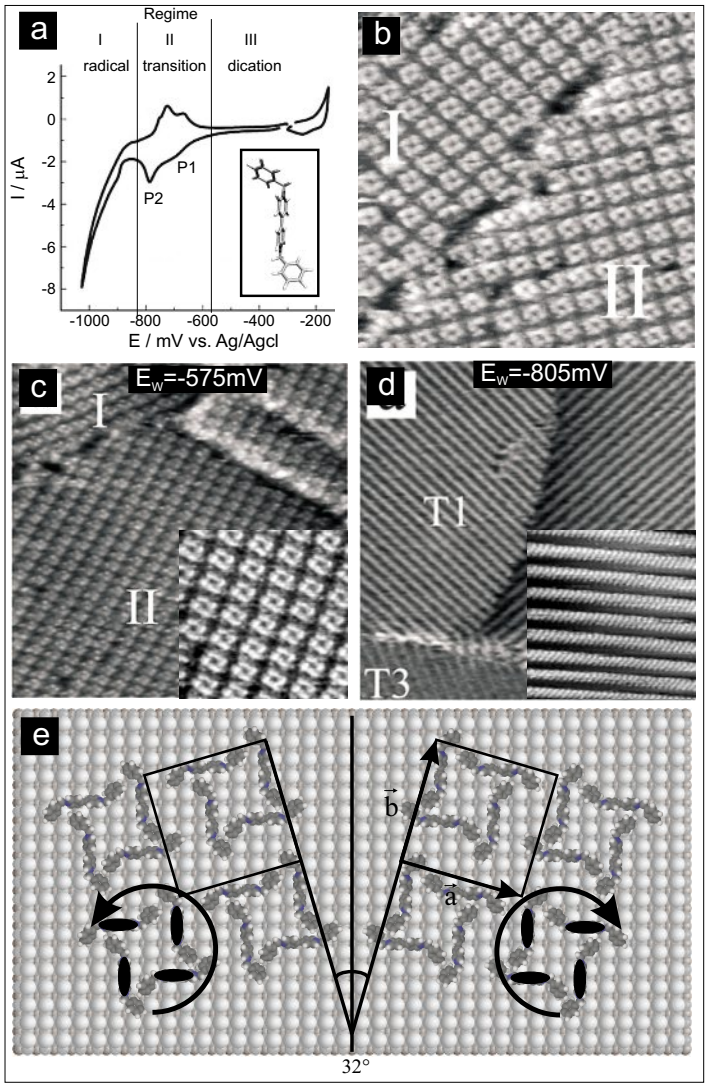

Fig. 12. Cyclic voltammogram of 0.1 mM DBV on a Cu(100) surface in 10 mM HCl (a), the inset shows the viologen molecule. Two mirror domains of the dication (b: 30 nm × 30 nm, EW = –400 mV vs. Ag/AgCl, IT = 0.25 nA, Ub = 86 mV), structure of the dication (c) and radical cation (d) (53 nm × 53 nm, IT = 0.1 nA, insets: 13 nm × 13 nm). Model of the cavitand structure with indicated rotational chirality (e).

affects the contribution of surface and adsorbate to the composite STM image, but also the decrease in bias combined with an increase in tunneling current causes the tip to scan closer to the surface so that the layer of organic molecules is removed by the STM tip and readsorbed only after the tip is again retracted by restoring the original tunneling parameters. The comparison of the substrate and the adsorbate image then shows that the cavitand structure is described by a $\begin{pmatrix} 2 & 7 \\ \bar{7} & 2 \end{pmatrix}$ matrix related to the chloride lattice (see the model in Fig. 12e). The peak P1 in the cyclic voltammogram in Fig. 12a indicates the reduction of the dication DBV^{2+} to the radical cation $DBV^{\bullet+}$. In the STM this is accompanied by a change in the surface structure of the organic phase, which now shows a stripe structure which arises from a well-known π-stacking of bipyridinium radicals as depicted in Fig. 12d, within the stripes the separation of adjacent molecules is 0.35 nm.

This shows that it is possible to change the redox state of the adsorbed organic species by variation of the electrode potential and to observe the changes induced thereby in the STM.

4. Conclusion

The electrochemical STM has become an invaluable tool for local probe microscopy and analysis of structure and phase behavior at electrified solid–liquid interfaces. Its capability to image surfaces during potential changes of the electrode allows observation of corrosion, deposition and electron transfer processes, while the spectroscopic abilities of the STM allow correlation of substrate and adsorbate structures as well as imaging different molecular orbitals (HOMO-LUMO) of adsorbed molecules. A new addition to the spectrum of possibilities is the development of an *in situ* video STM that allows not only snapshots of the surface but the observation of slowly proceeding surface processes in real time.

Received: October 4, 2011

[1] G. Binnig, H. Rohrer, *Helv. Phys. Acta* **1982**, *55*, 128.
[2] G. Binnig, H. Rohrer, C. Gerber, E. Weibel, *Appl. Phys. Lett.* **1982**, *40*, 178.
[3] B. Drake, R. Sonnenfeld, J. Schneir, P. K. Hansma, G. Slough, R. V. Coleman, *Rev. Sci. Instrum.* **1986**, *57*, 441.
[4] R. Sonnenfeld, P. K. Hansma, *Science* **1986**, *232*, 211.
[5] P. Lustenberger, H. Rohrer, R. Christoph, H. Siegenthaler, *J. Electroanal. Chem. Interfacial Electrochem.* **1988**, *243*, 225.
[6] K. Itaya, E. Tomita, *Surf. Sci.* **1988**, *201*, L507.
[7] D. W. Suggs, A. J. Bard, *J. Phys. Chem.* **1995**, *99*, 8349.
[8] D. W. Suggs, A. J. Bard, *J. Am. Chem. Soc.* **1994**, *116*, 10725.
[9] J. Wiechers, T. Twomey, D. M. Kolb, R. J. Behm, *J. Electroanal. Chem.* **1988**, *248*, 451.
[10] O. M. Magnussen, J. Hotlos, G. Bettel, D. M. Kolb, R. J. Behm, *J. Vacuum Sci. Technol. B* **1991**, *9*, 969.
[11] F. Endres, *Phys. Chem. Chem. Phys.* **2001**, *3*, 3165.
[12] A. M. Bittner, J. Wintterlin, B. Beran, G. Ertl, *Surf. Sci.* **1995**, *335*, 291.
[13] A. M. Bittner, J. Wintterlin, G. Ertl, *J. Electroanal. Chem.* **1995**, *388*, 225.
[14] D. M. Kolb, R. Ullmann, T. Will, *Science* **1997**, *275*, 1097.
[15] T. Tansel, O. M. Magnussen, *Phys. Rev. Lett.* **2006**, *96*, 026101.
[16] O. M. Magnussen, J. Hagebock, J. Hotlos, R. J. Behm, *Faraday Discuss.* **1992**, *94*, 329.
[17] K. Sashikata, Y. Matsui, K. Itaya, M. P. Soriaga, *J. Phys. Chem.* **1996**, *100*, 20027.
[18] M. Wilms, M. Kruft, G. Bermes, K. Wandelt, *Rev. Sci. Instrum.* **1999**, *70*, 3641.
[19] M. Wilms, P. Broekmann, C. Stuhlmann, K. Wandelt, *Surf. Sci.* **1998**, *416*, 121.
[20] C. Li, I. Pobelov, T. Wandlowski, A. Bagrets, A. Arnold, F. Evers, *J. Am. Chem. Soc.* **2008**, *130*, 318.
[21] X. P. Gao, M. J. Weaver, *J. Am. Chem. Soc.* **1992**, *114*, 8544.
[22] H. Siegenthaler, in 'Scanning Tunneling Microscopy II', Eds. H. R. Wiesendanger, H.-J. Guntherodt, Springer, Berlin, **1992**, p. 7.
[23] J. Clavilier, R. Faure, G. Guinet, R. Durand, *J. Electroanal. Chem.* **1980**, *107*, 205.
[24] T. Dretschkow, D. Lampner, T. Wandlowski, *J. Electroanal. Chem.* **1998**, *458*, 121.
[25] D. Friebel, C. Schlaup, P. Broekmann, K. Wandelt, *Surf. Sci.* **2006**, *600*, 2800.
[26] W. Schmickler, *Chem. Rev. (Washington, DC, USA)* **1996**, *96*, 3177.
[27] K. L. Sebastian, G. Doyen, *Surf. Sci. Lett.* **1993**, *290*, L703.
[28] W. Schindler, M. Hugelmann, *Surf. Sci.* **2003**, *541*, L643.
[29] T. Wandlowski, G. Nagy, *Langmuir* **2003**, *19*, 10271.
[30] G. Binnig, D. P. E. Smith, *Rev. Sci. Instrum.* **1986**, *57*, 1688.
[31] J. Frohn, J. F. Wolf, K. Besocke, M. Teske, *Rev. Sci. Instrum.* **1989**, *60*, 1200.
[32] P. Broekmann, ‚Atomare Struktur und Dynamik von Kupfer/Elektrolyt-Grenzflächen', Dissertation, Rheinische Friedrich-Wilhelms-Universität, Bonn, **2000**.
[33] P. Broekmann, M. Wilms, A. Spaenig, K. Wandelt, *Prog. Surf. Sci.* **2001**, *67*, 59.
[34] P. Broekmann, N. T. M. Hai, K. Wandelt, *J. Appl. Electrochem.* **2006**, *36*, 1241.
[35] B. Obliers, M. Anastasescu, P. Broekmann, K. Wandelt, *Surf. Sci.* **2004**, *573*, 47.
[36] D. M. Kolb, *Prog. Surf. Sci.* **1996**, *51*, 109.
[37] D. Friebel, '*In situ* STM-Untersuchungen ultradünner Kupferchalkogenidfilme auf Au (1 1 1)-Elektrodenoberflächen, Dissertation', Rheinische Friedrich-Wilhelms-Universität, Bonn, **2007**.

[38] Y. Nakai, M. S. Zei, D. M. Kolb, G. Lehmpfuhl, *Berichte Der Bunsen-Gesellschaft-Phys. Chem. Chem. Phys*. **1984**, *88*, 340.
[39] O. M. Magnussen, J. Hotlos, R. J. Nichols, D. M. Kolb, R. J. Behm, *Phys. Rev. Lett.* **1990**, *64*, 2929.
[40] M. Nakamura, O. Endo, T. Ohta, M. Ito, Y. Yoda, *Surf. Sci.* **2002**, *514*, 227.
[41] M. F. Toney, J. N. Howard, J. Richer, G. L. Borges, J. G. Gordon, O. R. Melroy, D. Yee, L. B. Sorensen, *Phys. Rev. Lett.* **1995**, *75*. 4472.
[42] F. A. Möller, O. M. Magnussen, R. J. Behm, *Phys. Rev. B* **1995**, *51*, 2484.
[43] C. Schlaup, K. Wandelt, to be published.
[44] P. Broekmann, M. Wilms, M. Kruft, C. Stuhlmann, K. Wandelt, *J. Electroanal. Chem*. **1999**, *467*, 307.
[45] B. Obliers, P. Broekmann, K. Wandelt, *J. Electroanal. Chem*. **2003**, *554,* 183.
[46] N. T. M. Hai, 'Preparation and characterization of copper-iodide thin films and organic supramolecular layers at copper/electrolyte interfaces', Dissertation, Rheinische Friedrich-Wilhelms-Universität, Bonn, **2007**.
[47] M. Wilms, 'Potentiodynamische Rastertunnelmikroskopie an Fest/Flüssig-Grenzflächen: Apparative Entwicklung und Untersuchungen zur Sulfat-adsorption auf Cu (111)', Dissertation, Rheinische Friedrich-Wilhelms-Universität, Bonn, **1999**.
[48] P. Broekmann, A. Spaenig, A. Hommes, K. Wandelt, *Surf. Sci*. **2002**, *517*, 123.